Title	Interface charge engineering in AlTiO/AlGaN/GaN metal–insulator–semiconductor devices
Author(s)	Nguyen, Duong Dai; Suzuki, Toshi-kazu
Citation	Journal of Applied Physics, 127(9): 094501
Issue Date	2020-03-05
Type	Journal Article
Text version	publisher
URL	http://hdl.handle.net/10119/19950
Rights	Copyright (c) 2020 AIP Publishing. This article may be downloaded for personal use only. Any other use requires prior permission of the author and AIP Publishing. This article appeared in Duong Dai Nguyen, Toshi-kazu Suzuki; Interface charge engineering in AlTiO/AlGaN/GaN metal–insulator–semiconductor devices, Journal of Applied Physics, 5 March 2020; 127 (9): 094501 and may be found at https://doi.org/10.1063/1.5141399.
Description	

Journal of Applied Physics

RESEARCH ARTICLE | MARCH 05 2020

Interface charge engineering in AlTiO/AlGaN/GaN metal–insulator–semiconductor devices

Duong Dai Nguyen ; Toshi-kazu Suzuki

J. Appl. Phys. 127, 094501 (2020)
https://doi.org/10.1063/1.5141399

Journal of Applied Physics ARTICLE scitation.org/journal/jap

Interface charge engineering in AlTiO/AlGaN/GaN metal–insulator–semiconductor devices

Cite as: J. Appl. Phys. **127**, 094501 (2020); doi: 10.1063/1.5141399
Submitted: 5 December 2019 · Accepted: 18 February 2020 ·
Published Online: 5 March 2020

View Online Export Citation CrossMark

Duong Dai Nguyen and Toshi-kazu Suzuki[a)]

AFFILIATIONS

Center for Nano Materials and Technology, Japan Advanced Institute of Science and Technology (JAIST), 1-1 Asahidai, Nomi, Ishikawa 923-1292, Japan

[a)]**Author to whom correspondence should be addressed:** tosikazu@jaist.ac.jp

ABSTRACT

Toward interface charge engineering in AlTiO/AlGaN/GaN metal-insulator-semiconductor (MIS) devices, we systematically investigated insulator-semiconductor interface fixed charges depending on the composition of the AlTiO gate insulator obtained by atomic layer deposition. By evaluating the positive interface fixed charge density from the insulator-thickness dependence of the threshold voltages of the MIS devices, we found a trend that the interface fixed charge density decreases with the decrease in the Al composition ratio, i.e., increase in the Ti composition ratio, which leads to shallow threshold voltages. This trend can be attributed to the large bonding energy of O-Ti in comparison with that of O-Al and to consequent possible suppression of interface oxygen donors. For an AlTiO gate insulator with an intermediate composition, the MIS field-effect transistors exhibit favorable device characteristics with high linearity of transconductance. These results indicate a possibility of interface charge engineering using AlTiO, in addition to energy gap engineering and dielectric constant engineering.

I. INTRODUCTION

As a gate insulator of GaN-based metal-insulator-semiconductor (MIS) field-effect transistors (FETs), Al_2O_3,[1] HfO_2,[2,3] TaON,[4] AlN,[5–9] BN,[10,11] and so on have been employed and investigated. Although a wide energy gap E_g and a high dielectric constant k_{ins} are preferable for a gate insulator, a trade-off between E_g and k_{ins} generally exists for insulators.[12] Aluminum titanium oxide Al_xTi_yO (AlTiO), an alloy of Al_2O_3 ($E_g \sim 7$ eV, $k_{ins} \sim 10$) and TiO_2 ($E_g \sim 3$ eV, $k_{ins} \sim 60$) with physical properties between them, is a useful insulator to balance E_g and k_{ins}.[13–19] Since the physical properties of AlTiO can be controlled by controlling its composition, AlTiO can be applied to energy gap engineering (E_g control) and dielectric constant engineering (k_{ins} control). Although there still exists a trade-off between E_g and k_{ins}, we can choose an AlTiO composition according to applications, considering the trade-off.

On the other hand, at the interface between an oxide gate insulator and a negatively polarized semiconductor surface, such as a Ga-face (Al)GaN surface, positive fixed charges tend to be generated and to cancel the negative polarization charges.[20–29] The interface fixed charges strongly influence threshold voltages of GaN-based MIS devices; a higher positive interface fixed charge density leads a more negative threshold voltage, which is unfavorable for device applications. If we develop methods to suppress and control the positive interface fixed charges, the threshold voltage can be controlled by "interface charge engineering."[24] In particular, sufficient suppression of the interface fixed charges is very important for normally off operations of GaN-based MIS devices.[30,31] However, the control of the interface fixed charges is not sufficient, and their origin is not fully elucidated, even though the importance of oxygen donors[20] and/or nitrogen vacancies[32] is pointed out. Therefore, further studies on interface charge engineering for GaN-based MIS devices are desirable.

Previously, we reported that Al_xTi_yO gate insulators with a composition of $x/(x+y) = 0.73$ for AlGaN/GaN MIS devices lead to a suppressed positive interface fixed charge density in comparison with Al_2O_3 gate insulators,[33] although the suppression is not enough. This result suggests that AlTiO/(Al)GaN interface fixed charged densities can be controlled by the AlTiO composition, and AlTiO can be applied to interface charge engineering, in addition to energy gap engineering and dielectric constant engineering for GaN-based MIS devices. In this work, for AlTiO/AlGaN/GaN MIS devices, we systematically investigated insulator-semiconductor interface fixed charges depending on the composition of AlTiO obtained by atomic layer deposition (ALD). We evaluated the interface fixed charge density from the insulator-thickness dependence of the threshold voltages of the MIS devices and found a trend that the interface fixed charge density decreases with the decrease in the Al composition ratio, i.e., increase in the Ti composition ratio. Moreover, for an AlTiO gate insulator with an intermediate composition, we obtained favorable MIS-FET characteristics with high linearity of transconductance. These results indicate a possibility of interface charge engineering using AlTiO gate insulators for GaN-based MIS devices.

II. DEVICE FABRICATION

We fabricated AlTiO/AlGaN/GaN MIS devices from an AlGaN/GaN heterostructure grown by metal-organic vapor phase epitaxy on sapphire(0001). The heterostructure consists of, from the top, $Al_{0.27}Ga_{0.73}N$ (7 nm)/n-$Al_{0.27}Ga_{0.73}N$ (20 nm, Si doping concentration of $2 \times 10^{18}\,cm^{-3}$)/ $Al_{0.27}Ga_{0.73}N$ (3 nm)/GaN (3000 nm). The device fabrication process started from Ti/Al/Ti/Au Ohmic electrode formation. After surface cleaning using organic solvents, oxygen plasma ashing, and an ammonium-based solution, Al_xTi_yO gate insulators with several compositions and thicknesses were formed by ALD at 130 °C, using trimethylaluminum (TMA), tetrakis-dimethylamino titanium (TDMAT), and H_2O as precursors. Post-deposition annealing in H_2(10%)-Ar(90%) at 350 °C was carried out, followed by Ni/Au gate electrode formation completing the device fabrication. Figure 1 shows the schematic cross section and a top-view optical image of the fabricated AlTiO/AlGaN/GaN MIS devices.

For the ALD of Al_xTi_yO, in order to control the composition, we repeated alternate supply of l-cycle TMA-H_2O and m-cycle TDMAT-H_2O as shown in the inset of Fig. 2. One-cycle TMA-H_2O and TDMAT-H_2O, respectively, correspond to Al_2O_3 and TiO_2 of $\lesssim 1$ Å thickness. Thus, for small cycle numbers, Al_2O_3 or TiO_2 cannot cover the surface and forms random clusters rather than a definite layer. As a result, using a pair of small coprime integers (l, m), we obtain an alloy-like mixed oxide Al_xTi_yO; the Al_xTi_yO film is not a superlattice of Al_2O_3 and TiO_2 and forms an interface

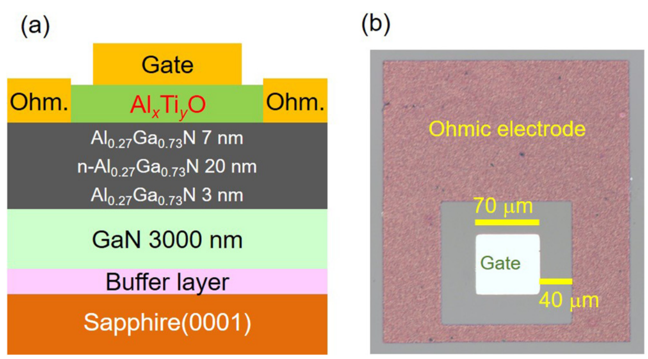

FIG. 1. (a) The schematic cross section and (b) a top-view optical image of the fabricated Al_xTi_yO/AlGaN/GaN MIS devices.

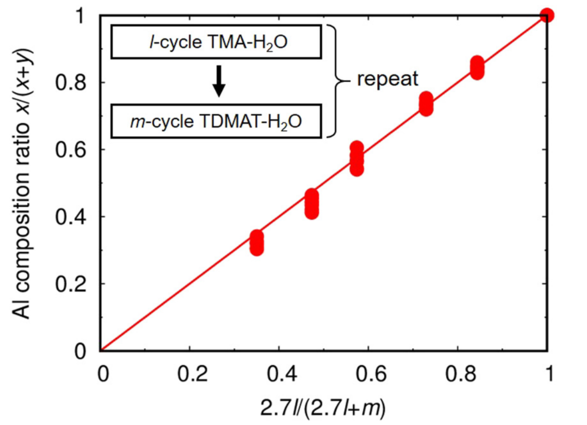

FIG. 2. Relation between the Al composition ratio $x/(x+y)$ and the set of cycle number (l, m).

with AlGaN as an alloy. It should be noted that $x + y \neq 1$ generally; the sum of the numbers of Al atoms and Ti atoms is not equal to the number of O atoms. Thus, we cannot use the notation of $Al_xTi_{1-x}O$ instead of Al_xTi_yO, and the composition is expressed by the Al composition ratio $x/(x+y)$. The compositions of the deposited Al_xTi_yO for $(l, m) = (1, 0)$, (2, 1), (1, 1), (1, 2), (1, 3), and (1, 5) were determined by x-ray photoelectron spectroscopy (XPS) measurements. We obtained the integral peak intensities (Al2s, Al2p) and (Ti2p, Ti3s, and Ti3p), and the composition was evaluated from their six intensity ratios. As a result, we find a good linear relation $x/y \simeq 2.7l/m$, i.e., $x/(x+y) \simeq 2.7l/(2.7l+m)$ as shown in Fig. 2, where the compositions of the deposited Al_xTi_yO are $x/(x+y) = 1.0$, 0.84, 0.73, 0.57, 0.47, and 0.35. The energy gaps of the deposited Al_xTi_yO were estimated by O1s XPS electron energy loss spectroscopy (EELS) as shown in the insets of Fig. 3, where the

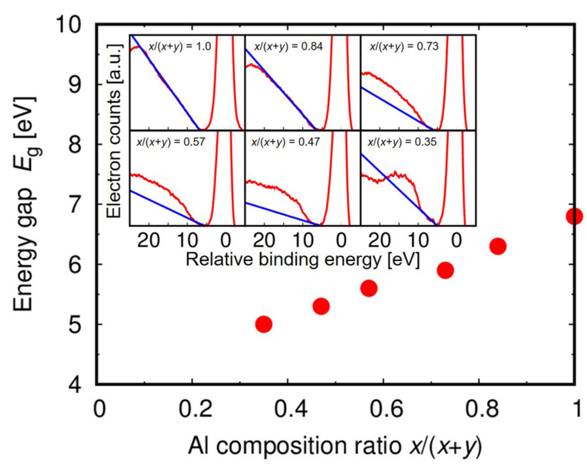

FIG. 3. The energy gap E_g of Al_xTi_yO depending on the Al composition ratio $x/(x+y)$. The inset shows XPS O1s EELS spectra used for the E_g estimation.

EELS spectra are plotted as functions of the relative binding energy to the O1s peak. The estimated energy gap E_g as a function of the Al composition ratio is shown in Fig. 3, where, as expected, E_g systematically decreases with a decrease in the Al composition ratio, i.e., with an increase in the Ti composition ratio. While the energy gap of the AlGaN is 4.2 eV, E_g for $x/(x+y) = 0.35$ is $\simeq 5$ eV, which may be not enough for a gate insulator. We consider that Al_xTi_yO with even a smaller Al composition ratio is not suitable for a gate insulator.

III. DEVICE CHARACTERIZATION

We measured the capacitance-voltage (C-V_G) characteristics of the AlTiO/AlGaN/GaN MIS devices with several AlTiO thicknesses $d_{ins} \leq 30$ nm, as shown in Fig. 4. The measurements were carried out at 1 MHz under V_G sweep from zero to negative voltages. By integrating C as a function of V_G, we obtained the sheet concentration of the two-dimensional electron gas (2DEG) n_s under the gate as shown in Fig. 5, from which the threshold voltage V_{th} can be determined.

Figure 6 shows the band diagram of the AlTiO/AlGaN/GaN MIS devices, assuming interface fixed charges. From this, we obtain

$$\frac{\sigma_{ins} + \sigma_D - \sigma_{GaN} - qn_s}{k_{ins}\varepsilon_0} d_{ins} + \frac{\sigma_{AlGaN} - \sigma_{GaN} - qn_s}{k_{AlGaN}\varepsilon_0} d_{AlGaN}$$
$$= \frac{\phi - \varphi - \Delta E_C}{q} - \frac{\sigma_D}{2k_{AlGaN}\varepsilon_0}(2d_{AlGaN} - d_D - 2d_S) + E_F/q - V_G$$
$$= \tilde{\psi}/q + E_F/q - V_G, \tag{1}$$

using the elementary charge $q > 0$; the vacuum permittivity ε_0; the insulator-semiconductor interface fixed charge density σ_{ins}; the polarization charge densities σ_{GaN} and σ_{AlGaN}; the sheet ionized

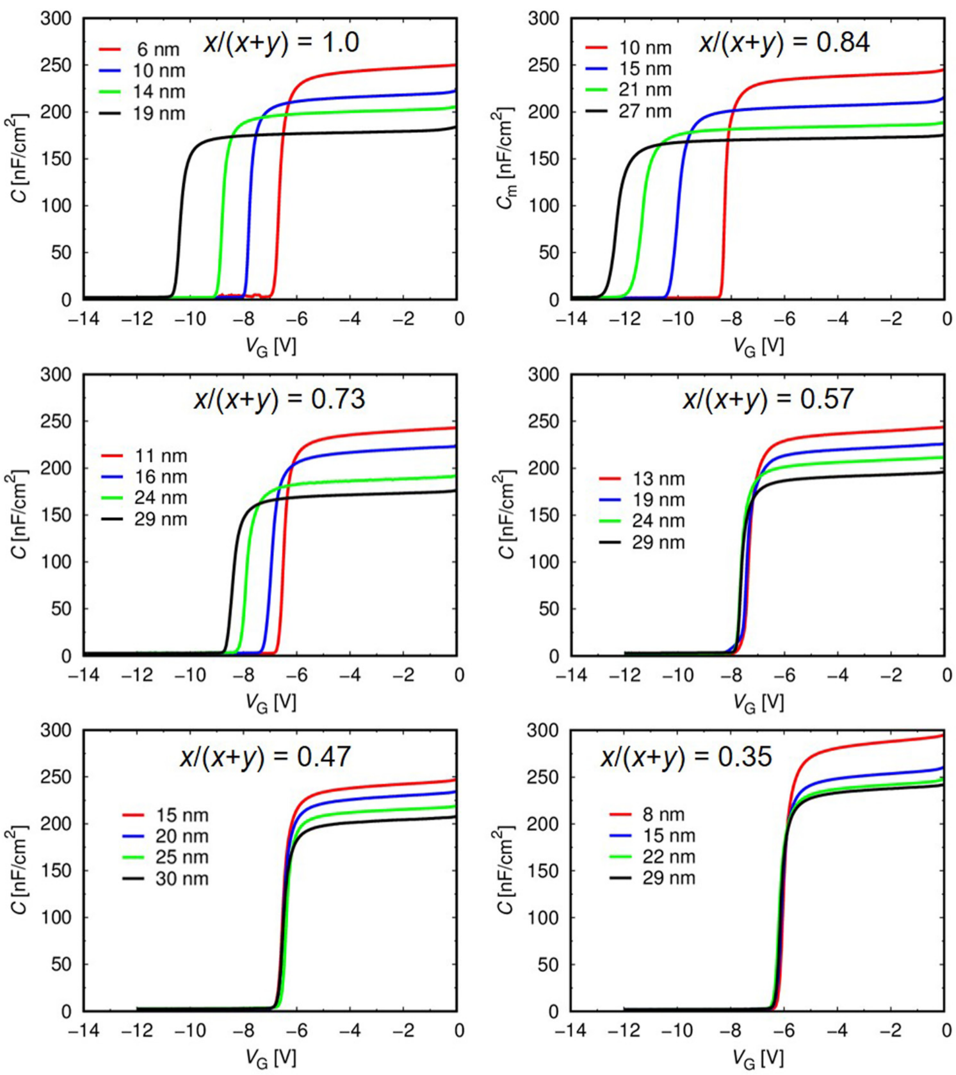

FIG. 4. C-V_G characteristics of the Al_xTi_yO/AlGaN/GaN MIS devices, measured at 1 MHz under V_G sweep from zero to negative voltages.

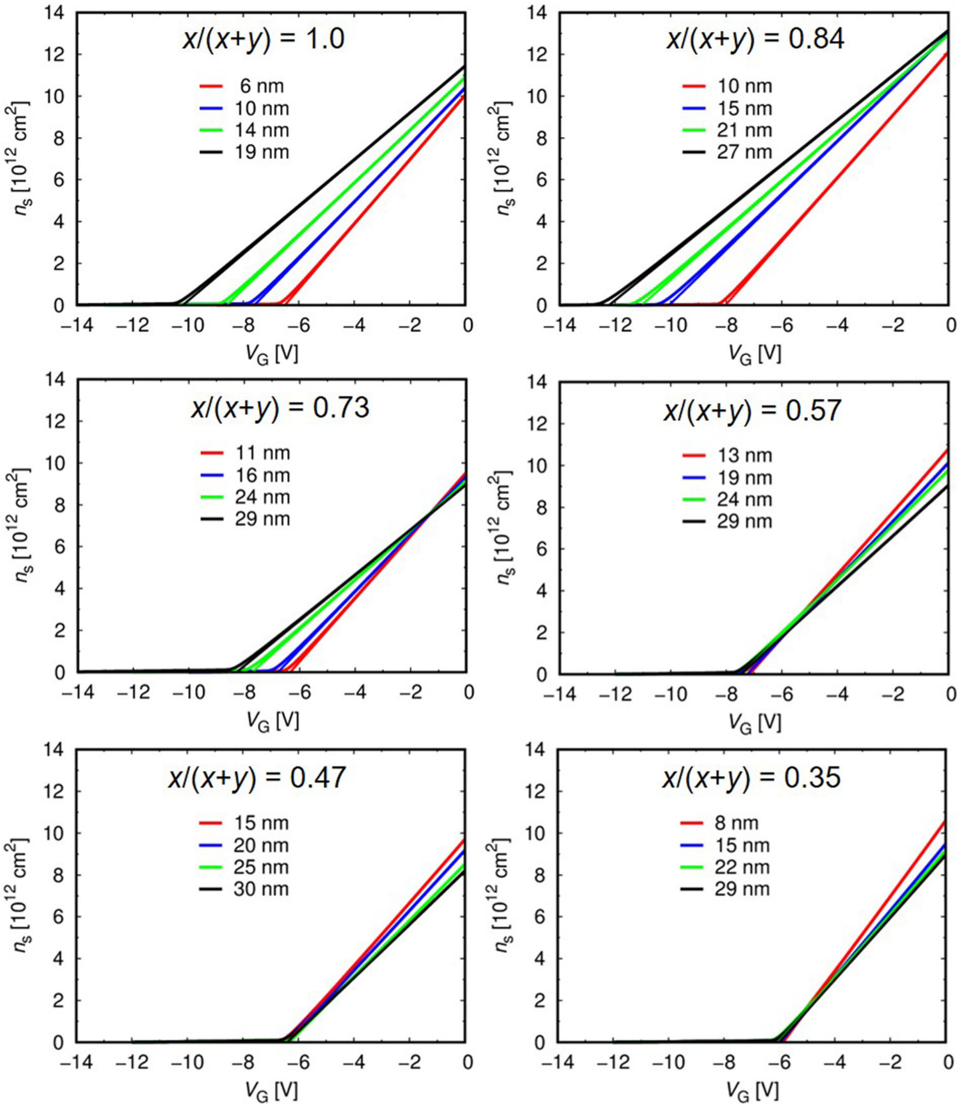

FIG. 5. The 2DEG sheet concentration n_s obtained by integrating C as functions of the gate voltage V_G.

donor density σ_D; the dielectric constants k_{ins} and k_{AlGaN}; the thicknesses d_{ins}, d_{AlGaN}, d_D, and d_S; the metal-insulator barrier height ϕ; the insulator-AlGaN conduction band offset φ; the AlGaN-GaN conduction band offset ΔE_C; and the 2DEG Fermi energy E_F, as defined in Fig. 6. Using the relation (1), the measurement results can be analyzed.

At $V_G = 0$ V, we obtain a capacitance given by

$$\frac{1}{C_0} \simeq \frac{d_{ins}}{k_{ins}\varepsilon_0} + \frac{d_{AlGaN}}{k_{AlGaN}\varepsilon_0} \tag{2}$$

from (1). Figure 7(a) shows the measured $1/C_0$ as functions of d_{ins}, where the linear relation (2) can be confirmed. From the fittings, we estimated dielectric constants $k_{AlGaN} \simeq 10$ and k_{ins} depending on the composition as summarized in Fig. 7(b). As expected, k_{ins} decreases with a decrease in the Al composition ratio, i.e., with an increase in the Ti composition ratio. The inset of Fig. 7(b) shows the correlation between E_g and k_{ins} of Al_xTi_yO, illustrating the trade-off. This confirms that we can control Al_xTi_yO insulator properties by controlling its composition, which is useful to balance E_g and k_{ins}.

At the threshold voltage $V_G = V_{th}$, since $n_s = 0$ and $E_F = 0$, the relation (1) gives

$$V_{th} = -\frac{\Delta\sigma_{ins}}{k_{ins}\varepsilon_0} d_{ins} - \frac{\Delta\sigma_{AlGaN}}{k_{AlGaN}\varepsilon_0} d_{AlGaN} + \tilde{\psi}/q, \tag{3}$$

where $\Delta\sigma_{ins} = \sigma_{ins} + \sigma_D - \sigma_{GaN}$ and $\Delta\sigma_{AlGaN} = \sigma_{AlGaN} - \sigma_{GaN}$. Since V_{th} is a linear function of d_{ins} with a slope of $-\Delta\sigma_{ins}/(k_{ins}\varepsilon_0)$, $\Delta\sigma_{ins}$ can be evaluated by the slope of the V_{th}-d_{ins}

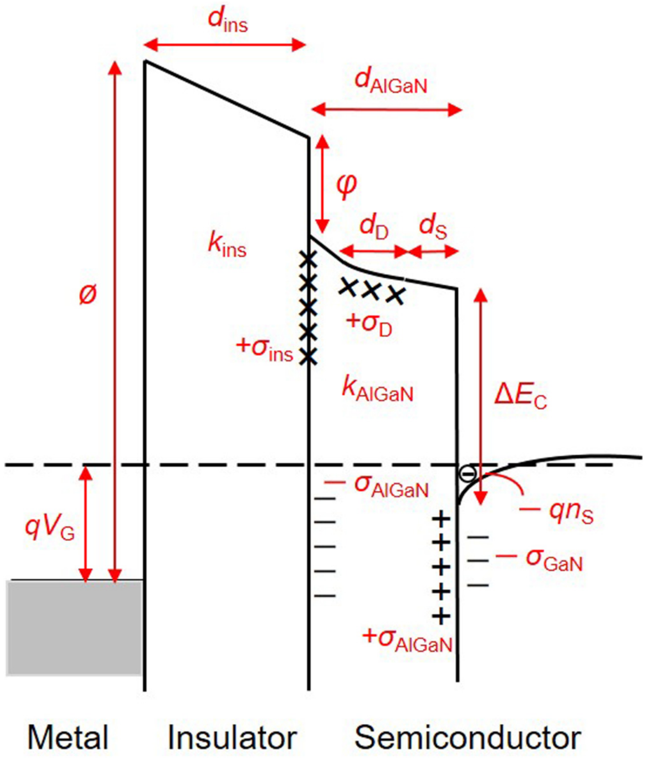

FIG. 6. The band diagram of the Al_xTi_yO/AlGaN/GaN MIS devices assuming interface fixed charges.

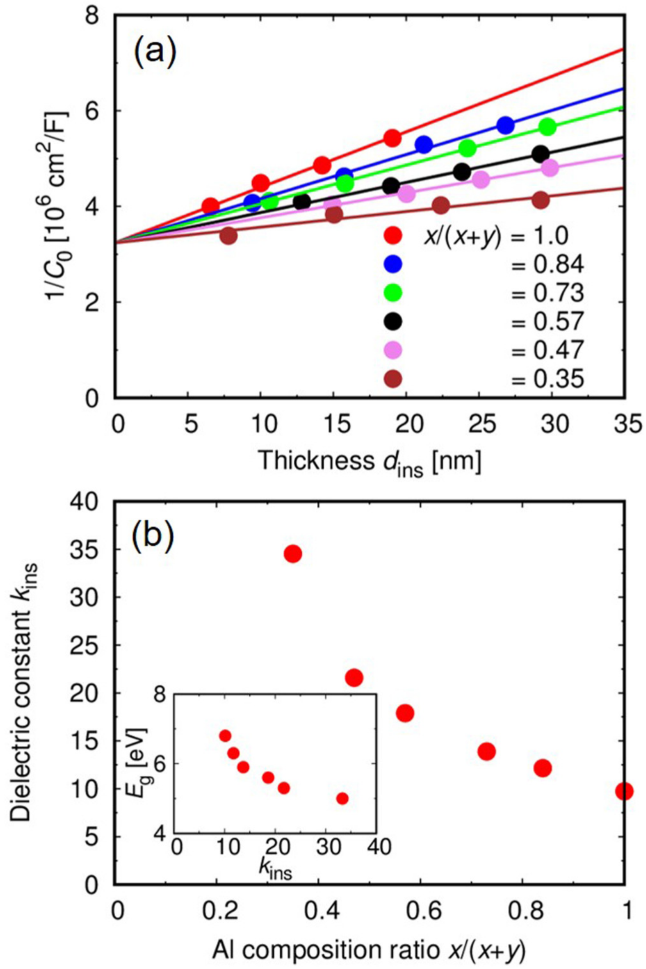

FIG. 7. (a) $1/C_0$ as linear functions of d_{ins} with fitting lines. (b) The dielectric constant k_{ins} of Al_xTi_yO depending on the Al composition ratio $x/(x+y)$. The inset shows the correlation between E_g and k_{ins}.

relation. Figure 8(a) shows the measured V_{th} as functions of d_{ins}. The linear relation (3) is obtained, indicating that V_{th} is dominated by the interface fixed charges (effects of bulk fixed charges in AlTiO are insignificant). We find a trend that, as the Al composition ratio decreases, the slope is positively shifted, suggesting that $\Delta\sigma_{ins}$ is reduced, i.e., the σ_{ins} is suppressed. In addition, we observe almost flat V_{th}-d_{ins} lines below intermediate Al compositions, indicating that the interface fixed charges are not further suppressed. From the fitting of V_{th}-d_{ins} using the relation (3), we obtain $\Delta\sigma_{ins}/q$. Even though $\Delta\sigma_{ins}$ is obtained experimentally, in order to evaluate σ_{ins}, it is necessary to assume σ_{GaN} and σ_{AlGaN}. If we assume $\sigma_{GaN}/q = 2.1 \times 10^{13}\,\mathrm{cm}^{-2}$ and $\sigma_{AlGaN}/q = 3.4 \times 10^{13}\,\mathrm{cm}^{-2}$,[34–38] using $\sigma_D/q = 4 \times 10^{12}\,\mathrm{cm}^{-2}$, we obtain Fig. 8(b) plotting σ_{ins} as a function of the Al composition ratio $x/(x+y)$, where the black dotted line corresponds to the neutral AlTiO/AlGaN interface. Three sigma error bars are included based on the asymptotic standard errors in the fitting of V_{th}-d_{ins}. We find a trend that, with a decrease in the Al composition ratio, i.e., an increase in the Ti composition ratio, the interface fixed charge density decreases and the AlTiO/AlGaN interface becomes more negatively charged, while the trend is saturated below intermediate Al compositions. This could be attributed to the difference between bonding energies of O-Ti and O-Al. Since the bonding energy of O-Ti (6.9 eV) is larger than that of O-Al (5.2 eV) and that of O-Ga (3.9 eV),[39] the incorporation of Ti can suppress bonding of oxygen with AlGaN at the interface, where oxygen bonded with Ga or Al at the interface may act as a donor.[20] As a result, positively ionized donors at the interface can be suppressed by Ti; i.e., the positive interface fixed charge density can be reduced. From the deposition rate of the AlTiO layer, we find that one-cycle TDMAT-H_2O gives a ~ 0.35 monolayer of TiO_2; as a result, for $m \geq 3$ or $x/(x+y) \leq 0.47$, the Ti density at the interface will be saturated, leading to the saturated trend. Although the origin of the interface fixed charges is not fully understood, the fact that they can be modulated by the AlTiO composition strongly suggests that the origin is oxygen donors rather than intrinsic polarization self-compensation.[40] Thus, further reduction of the interface fixed charge density will be in principle possible

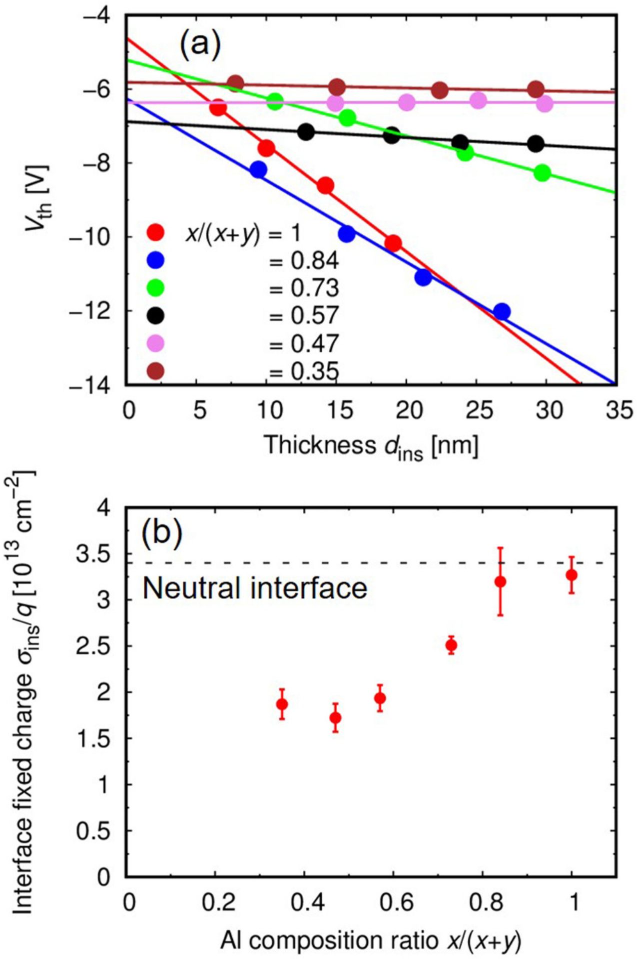

FIG. 8. (a) V_{th} of the Al_xTi_yO/AlGaN/GaN MIS devices as functions of d_{ins} with fitting lines. (b) The interface fixed charge density σ_{ins} depending on the Al composition ratio $x/(x+y)$. The black dotted line corresponds to the neutral AlTiO/AlGaN interface.

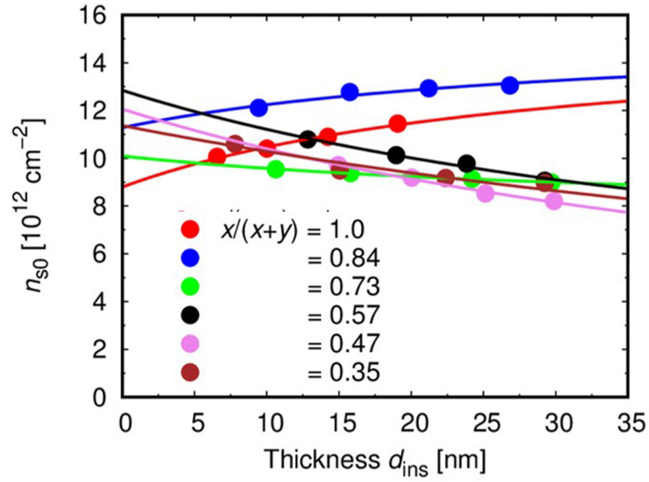

FIG. 9. n_{s0} of the Al_xTi_yO/AlGaN/GaN MIS devices as functions of d_{ins} with fitting curves.

independently of the polarization charge density.[41] We suppose that the oxygen donors have shallow energy levels, such as an energy depth of ~ 30 meV,[42] and are fully ionized. Thus, we consider that the modulation of the positive interface fixed charge density is that of the oxygen donor density itself, not owing to electrons trapped at deep interface states.[33]

The 2DEG density at $V_G = 0$ is given by

$$qn_{s0} \simeq \frac{\Delta\sigma_{ins} d_{ins}/(k_{ins}\varepsilon_0) + \Delta\sigma_{AlGaN} d_{AlGaN}/(k_{AlGaN}\varepsilon_0) - \tilde{\psi}/q}{d_{ins}/(k_{ins}\varepsilon_0) + d_{AlGaN}/(k_{AlGaN}\varepsilon_0)}. \quad (4)$$

It should be noted that the derivative is

$$\frac{\partial n_{s0}}{\partial d_{ins}} \simeq \frac{C_0}{k_{ins}\varepsilon_0}(\Delta\sigma_{ins}/q - n_{s0}), \quad (5)$$

whose sign depends on the difference between $\Delta\sigma_{ins}/q$ and n_{s0}. Figure 9 shows the experimental n_{s0}-d_{ins} with fitting curves using the relation (4), where the necessary fitting parameters have already been obtained by the fitting of V_{th}-d_{ins} using the relation (3). According to (5), n_{s0} is an increasing function of d_{ins} for $x/(x+y) = 1.0$ and 0.84, while $x/(x+y) \leq 0.73$ gives a decreasing function. For low interface fixed charge densities, the decreasing behavior has been simulated in Ref. 20.

Using the experimental results, we estimated the band diagrams of the AlTiO/AlGaN GaN MIS devices using the Poisson-Schrödinger calculation. For the calculation, the metal-AlTiO barrier height ϕ and the AlTiO-AlGaN conduction band offset φ are needed. Using the electron affinities ~ 1.9 eV of ALD-deposited Al_2O_3[43] and ~ 4.0 eV of ALD-deposited TiO_2,[44] we assume a linearly interpolated electron affinity $\sim [4.0 - 2.1x/(x+y)]$ eV of Al_xTi_yO. If there is no vacuum level discontinuity at the AlTiO/AlGaN, the AlGaN electron affinity ~ 3.5 eV (the GaN electron affinity ~ 4.1 eV) leads to the AlTiO-AlGaN conduction band offset $\varphi \simeq [x/(x+y) \times 2.1 - 0.5]$ eV. Since we experimentally obtained $\phi - \varphi$ from the V_{th}-d_{ins} fitting based on (3), ϕ can be obtained by using the above φ. The calculated band diagrams are shown in Fig. 10. The AlTiO/AlGaN interface is negatively charged by the incorporation of Ti. For $x/(x+y) = 0.35$, the AlTiO-AlGaN conduction band offset is $\varphi < 0.25$ eV, which is not enough for a gate insulator of AlGaN/GaN MIS devices. On the other hand, we consider that the AlTiO-AlGaN conduction band offset $\varphi \simeq 0.5$ eV for $x/(x+y) = 0.47$ can be used for a gate insulator.

In order to investigate the possibility of the AlTiO gate insulator with the composition $x/(x+y) = 0.47$ ($E_g \simeq 5.3$ eV and $\varphi \simeq 0.5$ eV), we fabricated and characterized AlTiO/AlGaN/GaN MIS-FETs using this composition and an insulator thickness of 20 nm. Figure 11 shows output and transfer characteristics of the device with a gate length $L_G = 1.4\,\mu$m, a source-gate distance of

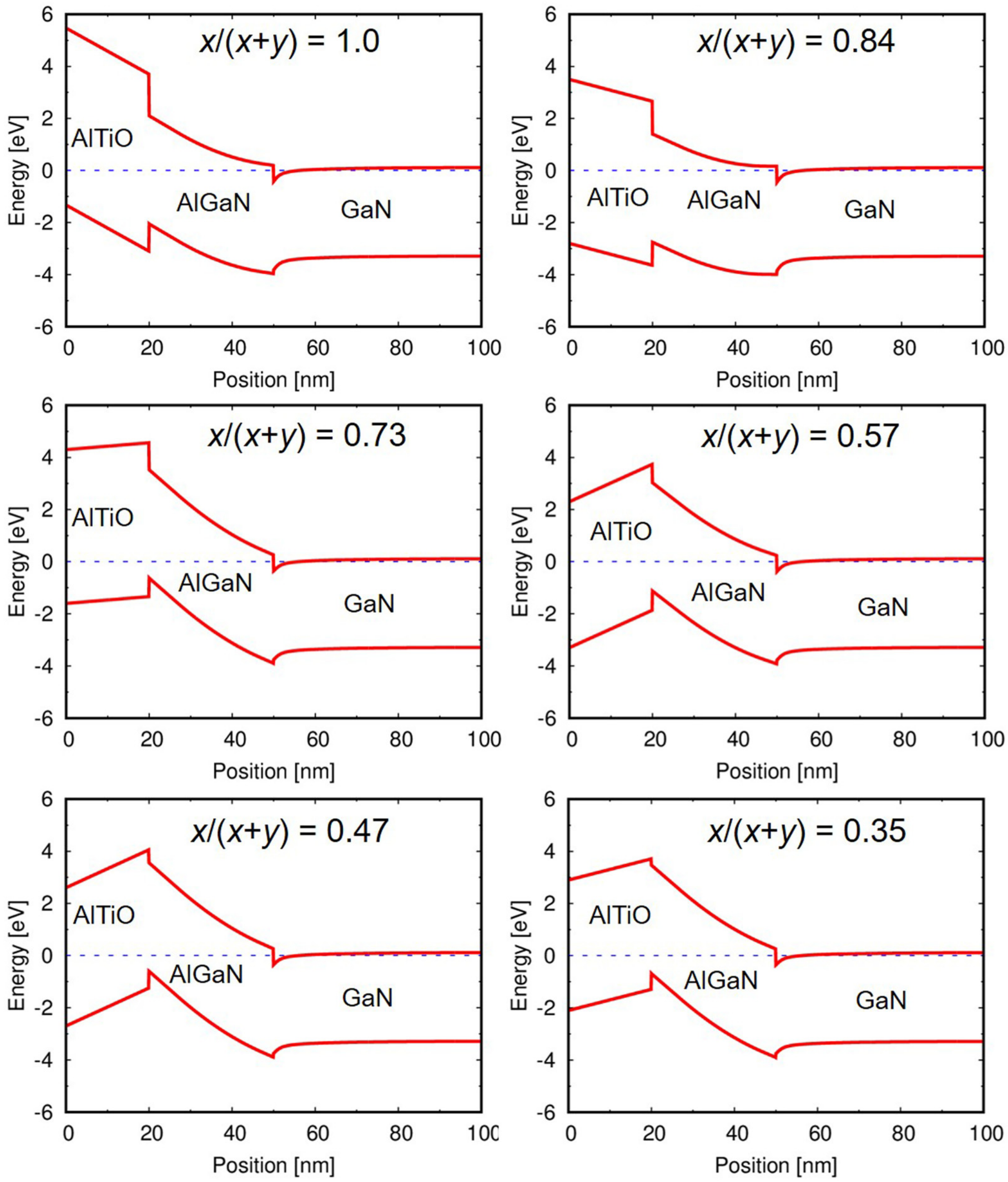

FIG. 10. The band diagrams of the Al_xTi_yO/AlGaN/GaN MIS devices obtained by the Poisson-Schrödinger calculation.

0.6 μm, a gate-drain distance of 2.5 μm, and a channel width of 50 μm, where the drain current I_D, gate current I_G, and transconductance g_m are normalized by the channel width. We find favorable FET characteristics. The output characteristics shown in Fig. 11(a) exhibit drain currents as high as ~ 900 mA/mm. The transfer characteristics at $V_D = 10$ V in the saturation regime, shown in Fig. 11(b), exhibit a low minimum sub-threshold swing of ~ 80 mV/decade and relatively low leakage currents. Although the leakage current level is two orders higher than that for typical Al_2O_3 gate insulators, the device has an on-off current ratio of $\sim 4 \times 10^7$, which is acceptable for many realistic applications. Moreover, from g_m-V_G characteristics, we find a peak $g_m \sim 110$ mS/mm with a full width half maximum (FWHM) as large as 9.6 V. Since the equivalent oxide thickness (AlGaN + AlTiO) is 14.8 nm, the FWHM is well above the guideline given in Ref. 45. In addition, the "gate voltage swing of g_m" (the gate voltage range where g_m remains ≥ 80% of the peak value)[46] is as large as 6.2 V. These indicate a very good linearity of the observed g_m.

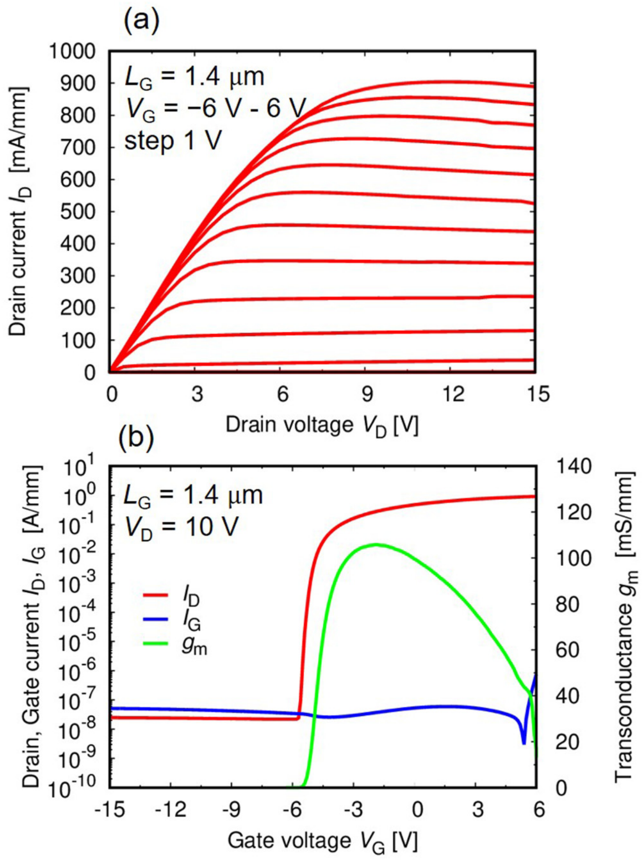

FIG. 11. (a) Output characteristics and (b) transfer characteristics at $V_D = 10$ V of the Al_xTi_yO/AlGaN/GaN MIS-FET with $x/(x+y) = 0.47$ and $L_G = 1.4$ μm. The drain current I_D, gate current I_G, and transconductance g_m are normalized by the channel width.

The obtained device characteristics suggest that Al_xTi_yO with the composition $x/(x+y) = 0.47$ can be a good high-k gate insulator for GaN-based MIS-FETs.

IV. CONCLUSION

We systematically investigated the insulator-semiconductor interface fixed charges in AlTiO/AlGaN/GaN MIS devices depending on the AlTiO composition. We found a trend that the interface fixed charge density decreases with a decrease in the Al composition ratio, i.e., increase in the Ti composition ratio, although the trend is saturated below intermediate Al compositions. The trend can be attributed to the large bonding energy of O-Ti in comparison with that of O-Al and to possible suppression of interface oxygen donors. Moreover, using the AlTiO gate insulators of the Al composition ratio $x/(x+y) = 0.47$, we obtained favorable MIS-FET characteristics with high linearity of transconductance. We consider that AlTiO can be utilized for interface charge engineering, in addition to energy gap engineering and dielectric constant engineering.

ACKNOWLEDGMENTS

We would like to thank K. Uryu for a helpful discussion.

REFERENCES

[1] T. Hashizume, S. Ootomo, and H. Hasegawa, Appl. Phys. Lett. **83**, 2952 (2003).
[2] C. Liu, E. F. Chor, and L. S. Tan, Appl. Phys. Lett. **88**, 173504 (2006).
[3] A. Kawano, S. Kishimoto, Y. Ohno, K. Maezawa, T. Mizutani, H. Ueno, T. Ueda, and T. Tanaka, Phys. Status Solidi C **4**, 2700 (2007).
[4] T. Sato, J. Okayasu, M. Takikawa, and T. Suzuki, IEEE Electron Device Lett. **34**, 375 (2013).
[5] Y. Liu, J. Bardwell, S. McAlister, S. Rolfe, H. Tang, and J. Webb, Phys. Status Solidi C **0**, 69 (2003).
[6] H.-A. Shih, M. Kudo, M. Akabori, and T. Suzuki, Jpn. J. Appl. Phys. **51**, 02BF01 (2012).
[7] H.-A. Shih, M. Kudo, and T. Suzuki, Appl. Phys. Lett. **101**, 043501 (2012).
[8] H.-A. Shih, M. Kudo, and T. Suzuki, J. Appl. Phys. **116**, 184507 (2014).
[9] S. P. Le, T. Q. Nguyen, H.-A. Shih, M. Kudo, and T. Suzuki, J. Appl. Phys. **116**, 054510 (2014).
[10] J.-C. Gerbedoen, A. Soltani, M. Mattalah, M. Moreau, P. Thevenin, and J.-C. D. Jaeger, Diam. Relat. Mater. **18**, 1039 (2009).
[11] T. Q. Nguyen, H.-A. Shih, M. Kudo, and T. Suzuki, Phys. Status Solidi C **10**, 1401 (2013).
[12] J. Robertson, Rep. Prog. Phys. **69**, 327 (2006).
[13] C. Mahata, S. Mallik, T. Das, C. K. Maiti, G. K. Dalapati, C. C. Tan, C. K. Chia, H. Gao, M. K. Kumar, S. Y. Chiam, H. R. Tan, H. L. Seng, D. Z. Chi, and E. Miranda, Appl. Phys. Lett. **100**, 062905 (2012).
[14] E. Miranda, J. Suñé, T. Das, C. Mahata, and C. K. Maiti, J. Appl. Phys. **112**, 064113 (2012).
[15] T. Ui, M. Kudo, and T. Suzuki, Phys. Status Solidi C **10**, 1417 (2013).
[16] S. P. Le, T. Ui, T. Q. Nguyen, H.-A. Shih, and T. Suzuki, J. Appl. Phys. **119**, 204503 (2016).
[17] A. Colon, L. Stan, R. Divan, and J. Shi, J. Vac. Sci. Technol. A **35**, 01B132 (2017).
[18] Z. Yatabe, K. Nishiyama, T. Tsuda, K. Nishimura, and Y. Nakamura, Jpn. J. Appl. Phys. **58**, 070905 (2019).
[19] S. Dutta Gupta, A. Soni, V. Joshi, J. Kumar, R. Sengupta, H. Khand, B. Shankar, N. Mohan, S. Raghavan, N. Bhat, and M. Shrivastava, IEEE Trans. Electron Devices **66**, 2544 (2019).
[20] S. Ganguly, J. Verma, G. Li, T. Zimmermann, H. Xing, and D. Jena, Appl. Phys. Lett. **99**, 193504 (2011).
[21] M. Esposto, S. Krishnamoorthy, D. N. Nath, S. Bajaj, T.-H. Hung, and S. Rajan, Appl. Phys. Lett. **99**, 133503 (2011).
[22] M. Ťapajna and J. Kuzmík, Appl. Phys. Lett. **100**, 113509 (2012).
[23] J. Son, V. Chobpattana, B. M. McSkimming, and S. Stemmer, Appl. Phys. Lett. **101**, 102905 (2012).
[24] T.-H. Hung, S. Krishnamoorthy, M. Esposto, D. N. Nath, P. S. Park, and S. Rajan, Appl. Phys. Lett. **102**, 072105 (2013).
[25] M. Ťapajna, M. Jurkovič, L. Válik, Š. Haščík, D. Gregušová, F. Brunner, E.-M. Cho, T. Hashizume, and J. Kuzmík, J. Appl. Phys. **116**, 104501 (2014).
[26] M. Matys, B. Adamowicz, A. Domanowska, A. Michalewicz, R. Stoklas, M. Akazawa, Z. Yatabe, and T. Hashizume, J. Appl. Phys. **120**, 225305 (2016).
[27] M. Ťapajna, L. Válik, F. Gucmann, D. Gregušová, K. Frohlich, Š. Haščík, E. Dobročka, L. Tóth, B. Pécz, and J. Kuzmík, J. Vac. Sci. Technol. B **35**, 01A107 (2017).
[28] T. Sato, K. Uryu, J. Okayasu, M. Kimishima, and T. Suzuki, Appl. Phys. Lett. **113**, 063505 (2018).
[29] M. Ťapajna, J. Drobný, F. Gucmann, K. Hušeková, D. Gregušová, T. Hashizume, and J. Kuzmík, Mater. Sci. Semicond. Process **91**, 356 (2019).

[30] G. Dutta, S. Turuvekere, N. Karumuri, N. DasGupta, and A. DasGupta, IEEE Electron Device Lett. **35**, 1085 (2014).
[31] M. Blaho, D. Gregušová, Š. Haščík, M. Jurkovič, M. Ťapajna, K. Fröhlich, J. Dérer, J. F. Carlin, N. Grandjean, and J. Kuzmík, Phys. Status Solidi A **212**, 1086 (2015).
[32] Z. Yatabe, J. T. Asubar, T. Sato, and T. Hashizume, Phys. Status Solidi A **212**, 1075 (2015).
[33] S. P. Le, D. D. Nguyen, and T. Suzuki, J. Appl. Phys. **123**, 034504 (2018).
[34] F. Bernardini, V. Fiorentini, and D. Vanderbilt, Phys. Rev. B **63**, 193201 (2001).
[35] O. Ambacher, B. Foutz, J. Smart, J. R. Shealy, N. G. Weimann, K. Chu, M. Murphy, A. J. Sierakowski, W. J. Schaff, L. F. Eastman, R. Dimitrov, A. Mitchell, and M. Stutzmann, J. Appl. Phys. **87**, 334 (2000).
[36] J. A. Garrido, J. L. Sanchez-Rojas, A. Jimenez, E. Munoz, F. Omnes, and P. Gibart, Appl. Phys. Lett. **75**, 2407 (1999).
[37] E. J. Miller, E. T. Yu, C. Poblenz, C. Elsass, and J. S. Speck, Appl. Phys. Lett. **80**, 3551 (2002).
[38] A. T. Winzer, R. Goldhahn, G. Gobsch, A. Link, M. Eickhoff, U. Rossow, and A. Hangleiter, Appl. Phys. Lett. **86**, 181912 (2005).
[39] Y.-R. Luo, *Handbook of Bond Dissociation Energies in Organic Compounds* (CRC Press, 2002).
[40] E. Ber, B. Osman, and D. Ritter, IEEE Trans. Electron Devices **66**, 2100 (2019).
[41] F. Gucmann, M. Ťapajna, O. Pohorelec, Š. Haščík, K. Hušeková, and J. Kuzmík, Phys. Status Solidi A **215**, 1800090 (2018).
[42] K. Mochizuki, *Vertical GaN and SiC Power Devices* (Artech House, 2018).
[43] H. D. Trinh, M. T. Nguyen, Y. C. Lin, Q. V. Duong, H. Q. Nguyen, and E. Y. Chang, Appl. Phys. Express **6**, 061202 (2013).
[44] F. Marques and J. Jasieniak, Appl. Surf. Sci. **422**, 504 (2017).
[45] K. Nishiguchi, S. Kaneki, S. Ozaki, and T. Hashizume, Jpn. J. Appl. Phys. **56**, 101001 (2017).
[46] Z. H. Liu, G. I. Ng, S. Arulkumaran, Y. K. T. Maung, K. L. Teo, S. C. Foo, and V. Sahmuganathan, IEEE Electron Device Lett. **31**, 803 (2010).